IMPROVING THERMAL PERFORMANCE AND ENERGY PRODUCTION OF PHOTOVOLTAIC THERMAL COLLECTOR BY BIFURCATING TREE-LIKE COOLING CHANNELS

Long Zhang[1], Rui Chang[2], Chengbin Zhang[2], Cheng Yu[3*]

[1]Shandong Electric Power Engineering Consulting Institute Co., Ltd., Jinan, China

[2]School of Energy and Environment, Southeast University, Nanjing, China

[3]College of Electrical, Energy and Power Engineering, Yangzhou University, Yangzhou, China

[*] Corresponding author; E-mail: chengyu@yzu.edu.cn

Photovoltaic thermal collectors with cooling channels suffers from poor temperature uniformity and high heat loss at high radiation intensities. However, traditional cooling channels are unable to address these specific heat dissipation requirements. In this research, the photovoltaic/thermal collector within the nature-inspired bifurcating tree-like cooling channels is designed and compared with the traditional parallel cooling channels. A theoretical model for heat exchange in the photovoltaic/thermal collector is developed. The system's performance with different structural parameters is investigated. The results indicate that the nature-inspired bifurcating tree-like II-type cooling channel exhibits superior overall performance for the photovoltaic/thermal collector. Besides, the average photovoltaic module surface temperature drops by 12.47K and the system's electric efficiency rises by 0.84% by growing the inlet speed. Furthermore, the lowest pressure drops is 13.62Pa in the cooling channel when the number of grades is 4 and the inlet mass flow rate is 0.00256kg/s. With the number of grades increasing, the average temperature of the photovoltaic module reduces. When the channel bifurcation angle is 1.0α-type and the inlet mass flow rate is 0.0124kg/s the system's electric efficiency is 13.66% and the PV/T collector's performance is optimal.

Key words: *Photovoltaic/thermal; electric efficiency; numerical model*

1. Introduction

With the escalating crises of fossil fuel exhaustion and climate change over recent decades, the globe has been committed to the exploration of new energy resources[1-3]. Considered a primary clean and sustainable power source, solar energy has garnered international attention and received powerful policy support for the advancement of the photovoltaic (PV) field[4, 5]. PV is a technology that utilizes the PV influence of semiconductor modules to transmute solar energy into direct current electricity[6, 7]. For practical applications, the bulk of solar radiation is converted into heat energy, leading to the degradation of total system performance[8, 9]. Intending to improve its performance, the photovoltaic thermal (PV/T) collector combines thermal transfer tubes integrated with PV modules,

removing waste heat from PV modules by cooling fluid flow in the tubes, and improving the efficiencies of conventional PV systems[10, 11].

As a pivotal element of the PV/T collector, the cooling channels enable efficient absorption and conduct of the thermal production from the PV cells, thereby enhancing the thermal energy utilization of the PV/T collector[12]. There has been much research into the influence of cooling channels on PV/T collector. Candanedo et al[13]. utilized a computational fluid dynamics model to investigate the flow and thermal transport properties of an asymmetrically heated inclined duct that could be used in a building-integrated PV/T system. Cooling channels of two different configurations were developed. Shen et al[14], designed a cooling channel with a bionic shark dorsal fin-type slot to investigate the effects of solar radiation and inlet flow mass on the performance of PV/T collector system. The results show that the average surface temperature of PV modules with the optimal cooling channel is 6.05°C lower than the conventional cooling channel. Boumaaraf et al[15]. compared the output of the PV and the PV/T experimentally in certain weather situations by experiment. The study yielded electrical efficiencies of 7% for the conventional PV generator and 6.26% for the PV/T collector. Wang et al[16], experimentally explored a PV/T collector with an S-shaped cooling channel and investigated the effect of inlet flow rate on the performance of the PV/T collector. The experiments show that the system electrical efficiency is 14.71% and thermal efficiency is 56.79% when the inlet flow rate is 0.9 L/min. The above studies show that the use of cooling channels enhances the performance of the system. Nevertheless, due to the various constructions of cooling channels in PV/T collectors resulting differences in the pressure drop and cost. Therefore, enhancing the structural parameters of the cooling channel is vital for boosting the efficiency of the PV/T collector. Many scholars have researched the design optimization of cooling channel structures. Poredoš et al[17]. by numerical and experimental, examined the performance of systems with three types of channel shapes: serial, parallel and bionic. The bionic absorber achieved the lowest average effluent temperature of 44.1°C and the least pressure loss. Nahar et al[18]. examined the efficiency of a PV/T collector featuring a pancake-shaped channel. Numerical calculations show that the cell average temperature reduction for both copper and aluminum is approximately 42° as the inlet speed enhances 0.0009-0.05 m/s. Chaoqun et al[19]. established a model of thermal transport for PV/T collector within parallel cooling channel, which discussed the impact of the construction characteristics on the PV/T collector. When the number of subchannels is 10, the pressure gradient within the cooling channel is minimized. Shiqian et al[20]. presented and investigated a PV/T system that has a new graphite-embedded trapezoidal fluidic channel arranged in parallel S-shape. Compared to PV modules, the study showed a 12.7°C average daily decline in cell temperature and a 5.20% relative increase in power output. Xiangrui et al[21]. explored the theory of super-thin conductive heat absorbers with built-in corrugated channels. By discussing the effects of structural parameters like the number of corrugations and width of the flow channel on the PV/T collector performance. With the reduction of the runner absorbing plate width 4-3 mm, the heat collected increased by 18.6%. The above studies have the effect of different types of cooling channels on the performance of PV/T collector. Inspired by the bionic construction in nature, the bifurcating tree-like channel has recently been applied to various kinds of transport systems, like the heat sink, the microreactor, microfluidics, etc. and exhibits excellent performance[22-24]. Therefore, the utilization of bifurcating tree-like cooling channels within PV/T collector is conducive to achieving better thermal performance. Nevertheless, the effects of bifurcating tree-like cooling channels on the performance of PV/T collectors and the internal flow heat transfer characteristics are less understood.

In conclusion, the implementation of cooling channels has proven to enhance the performance of the PV/T collector. This investigation entails the development and comparison of the PV/T collector within nature-inspired bifurcating tree-like cooling channels against a traditional PV/T collector within parallel cooling channels. The heat transfer within a PV/T collector with bifurcating tree-like cooling channels is investigated theoretically. Numerical simulation is conducted on the PV/T collector to assess the impact of the bifurcating tree-like cooling channel architecture on its performance. The impact of design parameters on the PV/T collector is examined to refine the configuration of the bifurcating tree-like cooling channels. Aiming to further improve the performance and power generation of the PV/T collector.

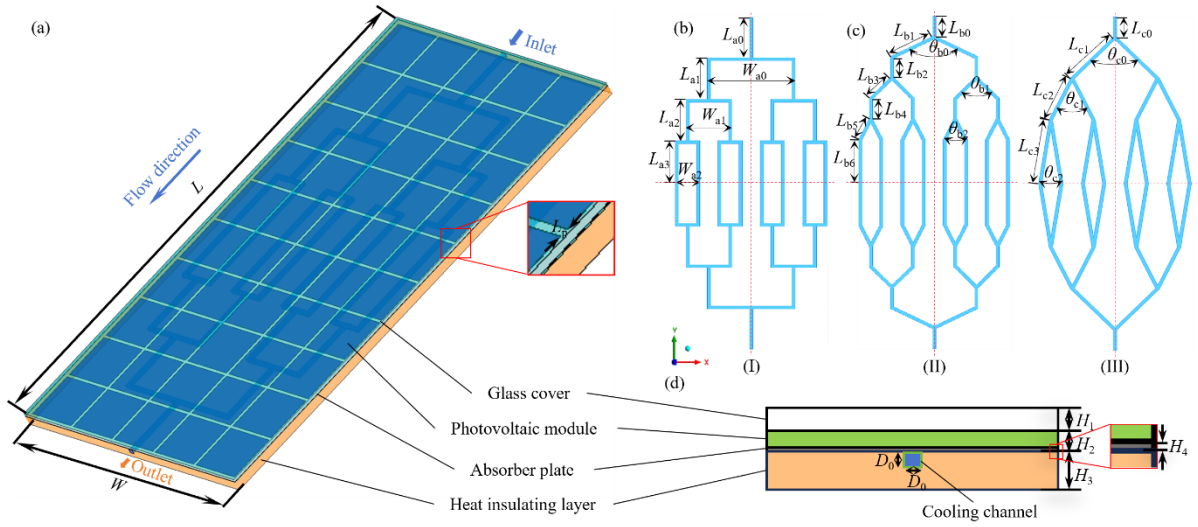

Figure 1 Diagram of the PV/T collector configuration within bifurcating tree-like cooling channels (a) the PV/T collector; (b) the conventional parallel cooling channels; (c) the bifurcating tree-like cooling channels; (d) the lateral view of the PV/T collector assembly.

2. Mathematical model

2.1. Physical model

This study employs numerical simulation to investigate the transfer of thermal energy in the system. Figure 1 shows the PV/T collector structure with bifurcating tree-like cooling channels. Figure 1 (b) displays the traditional parallel cooling channel. Figure 1 (c) illustrates the nature-inspired bifurcating tree-like cooling channels. The lateral view of the PV/T collector is presented in Figure 1 (d). The design data for the PV/T collector are specified in Table 1. The physical parameters for each material are shown in Table 2.To facilitate the mathematical calculations, the assumptions are made:(1) The process of heat transfer is in a steady state;(2) Transmissivity of ethylene vinyl acetate copolymer is considered 100%; (3) The heat dissipation from the base and flanks of the system is neglected.

Table 1 Dimensions of PV/T collector with different cooling channels.

Symbol	Instructions	Sizes/mm
L	Length of PV/T Collector	1074
W	Width of PV/T collector	544
H_1	Thickness of glass cover	6

H_2	Thickness of PV/T module	0.3
H_3	Insulation thickness	20
H_4	Thickness of absorber	1
D_0	Height of cooling channels	10
d_0	Thickness of cooling channel wall	1
L_p	Gaps between PV modules	6

(I) I-type cooling channel parameters in Figure 1(b)		(II) II-type cooling channel parameters in Figure 1(b)		(III) III-type cooling channel parameters in Figure 1(b)	
L/mm	W/mm	L/mm	θ/°	L/mm	θ/°
L_{a0} = 130	W_{a0} = 266	L_{b0} = 65	L_{b5} = 74.2	L_{c0} = 65	θ_{c0} = 88.2
L_{a1} = 134	W_{a1} = 138	L_{b1} = 143.6	L_{b6} = 139	L_{c1} = 183.9	θ_{c1} = 51.1
L_{a2} = 134	W_{a2} = 74	L_{b2} = 67	θ_{b0} = 126.2	L_{c2} = 148.5	θ_{c2} = 17.7
L_{a3} = 139	-	L_{b3} = 92.7	θ_{b1} = 87.4	L_{c3} = 208.5	-
-	-	L_{b4} = 67	θ_{b2} = 51.1	-	-

Table 2 Physical properties parameters of materials.

materials	ρ[kgm^{-3}]	c_p[Jkg^{-1}K^{-1}]	λ[Wm^{-1}K^{-1}]	ψ	α	ε
glass cover	2200	830	1	0.91	0.1	0.9
PV/T modules	2330	700	148	0.09	0.8	-
aluminium	2700	900	120	0	0.9	0.1
heat insulating layer	140	1220	0.035	-	-	-

2.2. Governing equations

The governing equations are given below.

Mass conservation equation：

$$\frac{\partial u}{\partial x}+\frac{\partial v}{\partial y}+\frac{\partial w}{\partial z}=0 \tag{1}$$

where u, v, w is the speed on the x, y, z coordinates, respectively.

Momentum equation:

$$\nabla\cdot(\rho u\vec{u})=-\frac{\partial p}{\partial x}+\frac{\partial \tau_{xx}}{\partial x}+\frac{\partial \tau_{yx}}{\partial y}+\frac{\partial \tau_{zx}}{\partial z} \tag{2}$$

$$\nabla\cdot(\rho v\vec{u})=-\frac{\partial p}{\partial y}+\frac{\partial \tau_{xy}}{\partial x}+\frac{\partial \tau_{yy}}{\partial y}+\frac{\partial \tau_{zy}}{\partial z} \tag{3}$$

$$\nabla\cdot(\rho w\vec{u})=-\frac{\partial p}{\partial z}+\frac{\partial \tau_{xz}}{\partial x}+\frac{\partial \tau_{yz}}{\partial y}+\frac{\partial \tau_{zz}}{\partial z}+F \tag{4}$$

where p is the pressure, τ is the viscous stress, F is the force of gravity, ρ is the water density.

Energy equation:

$$\frac{\partial(\rho uT)}{\partial x}+\frac{\partial(\rho vT)}{\partial y}+\frac{\partial(\rho wT)}{\partial z}=\frac{\partial}{\partial x}(\frac{k}{c_p}\frac{\partial T}{\partial x})+\frac{\partial}{\partial y}(\frac{k}{c_p}\frac{\partial T}{\partial y})+\frac{\partial}{\partial z}(\frac{k}{c_p}\frac{\partial T}{\partial z}) \tag{5}$$

where T is the water temperature, c_p is the thermal conductivity, k is the heat transfer coefficient.

Select the discrete ordinates radiation model for the computation of the radiative heat transfer inside the PV/T. The corresponding equation as below:

$$\nabla \cdot (I_\lambda(\vec{r},\vec{s})\vec{s}) + (\sigma_\lambda + \sigma_s) I_\lambda(\vec{r},\vec{s}) = \sigma_\lambda n^2 I_{b\lambda} + \frac{\sigma_s}{4\pi}\int_0^{4\pi} I_\lambda(\vec{r},\vec{s}')\Phi(\vec{s}\cdot\vec{s}')d\Omega' \quad (6)$$

where I_λ is the spectral intensity, $\vec{s}$ is the direction vector, $\vec{r}$ is the location vector, $\vec{s}'$ is the scattering direction, Φ is the phase function, $I_{b\lambda}$ is the radiation of the black body within a specific wavelength range per unit solid angle, σ_s is scattering coefficient, σ_λ is spectral absorption coefficient, Ω' is the solid angle.

Photovoltaic conversion efficiency η_e can be calculated as:

$$\eta_e = \eta_{swc}[1 - 0.0045(T_{cell} - 289.15)] \quad (8)$$

where η_{swc} = 0.15 is the PV conversion efficiency at standard conditions and T_{cell} is the average PV module temperature.

2.3. Boundary conditions and numerical solutions

Based on the hydraulic diameter of the cooling channel and other parameters, $R_e = \rho v d/\mu$ within the cooling channels is under 2000, so the flow in the cooling channels is laminar. This paper adopts the laminar flow three-dimensional steady-state model. The DO model is used for internal radiation heat transfer. At the inlet of the cooling channels is mass flow rate selected in intervals of 0.00128 kg/s from 0.00256 to 0.01024 kg/s, G = 1000 W/m^2. The water pressure at the outlet is set to gauge pressure 0 Pa. The local ambient temperature is 300 K. The outside ambient wind speed is 2 m/s. The cooling water inlet temperature is 300 K. Adiabatic boundary conditions are used for its bottom and sides. Both thermal convection and radiation exit the upper face of the glass cover, the heat transfer coefficient is 11.8 W/m$^2\cdot$K. The finite volume method is used to solve the above governing equations with the software Fluent 2022R1, The SIMPLE algorithm is used for the coupling of pressure and velocity, and the second-order windward difference format is used for solving the momentum and energy equations[19, 25].

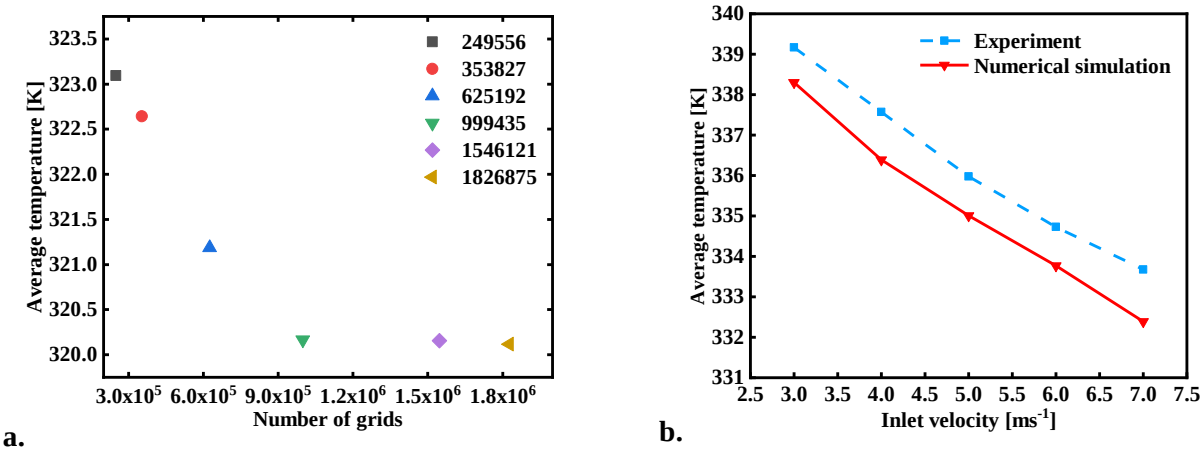

Figure 2 a. Grid-independent test and b. experimental verification[18].

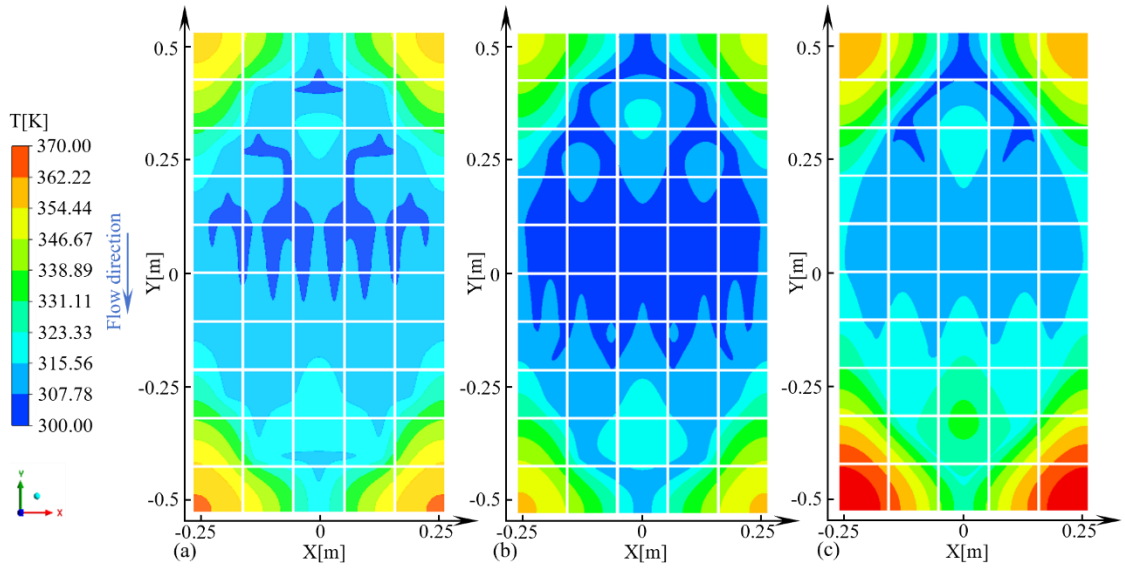

Figure 3 The distribution of temperature of PV modules with different cooling channel structures.

2.4. Validation

2.4.1 Grid independence test

This research conducts a grid-independence analysis. Figure 2(a) shows the grid-independent test, as the number of grids has escalated from 999435 to 1826875, the changes in average temperature are negligible. Consequently, when the number of grids exceeds 999435, difference in change between two adjacent data sets is less than 0.1K, the influence of the grid count on the outcomes diminishes significantly. In light of computational efficiency and precision, all simulation analyses conducted in this study are based on grid counts exceeding 999435.

2.4.2 Numerical model validity analysis

To ensure the precision of the numerical calculation approach, a physical model identical to that used by Nahar et al[18]. experiments are established in this investigation. The numerical simulations employ similar boundary conditions and material properties. The comparison between simulation and experiment is presented in Figure 2(b). The degree of fit between the experimental data and the simulated values is reflected by the root-mean-square deviation, which is closer to zero, indicating that the experimental data and the simulated values are fitted to a higher degree. The root mean square deviation is calculated as equation (9). The root-mean-square deviation of the simulated values from the experimental values is 5.81%. Therefore, in this investigation, this model enables the prediction of the performance of the PV/T collector.

$$RMSE = \sqrt{\frac{1}{M}\sum_{i=1}^{M}\left(\frac{(X_{sim,i} - X_{\exp,i})^2}{X_{\exp,i}}\right)} \times 100\% \quad (9)$$

Where $X_{\mathrm{sim,i}}$ represents the simulated value and $X_{\mathrm{exp,i}}$ represents the experimentally obtained value, M is the number of data.

3. Results and discussions

3.1. Comparison between parallel cooling channels and bifurcating tree-like cooling channels

The configuration of the bifurcating tree-like has a major implication on the overall thermal transmission properties of the cooling channels. Figure 1(b) and (c) depict the traditional parallel and the nature-inspired bifurcating tree-like cooling channels, respectively. This portion researches the heat transfer properties of the traditional parallel and nature-inspired bifurcating tree-like cooling channels to determine the system's properties.

Figure 3 illustrates the temperature distribution across the PV module featuring various bifurcating tree-like structures (v_{in} = 0.01024 kg/s). As shown in Figure 3, the lowest temperatures are 303.30 K, 302.36 K, and 305.73 K, in that order. However, in Figure 3(c), there is a significant high-temperature region near the outlet with maximum temperatures of 366.17 K. Besides, the larger the heat transfer area heat transfer rises, the III-type cooling channel area accounted for the smallest area of the PV module, thus the corner heat cannot be sufficiently cooled, the temperature uniformity of the performance degradation. Therefore, the thermal uniformity in (b) is better than (a) and (c). Also, the nature-inspired bifurcating tree-like II-type cooling channel exhibits enhanced thermal conductivity compared to the I-type and III-type channels, facilitating more effective heat absorption.

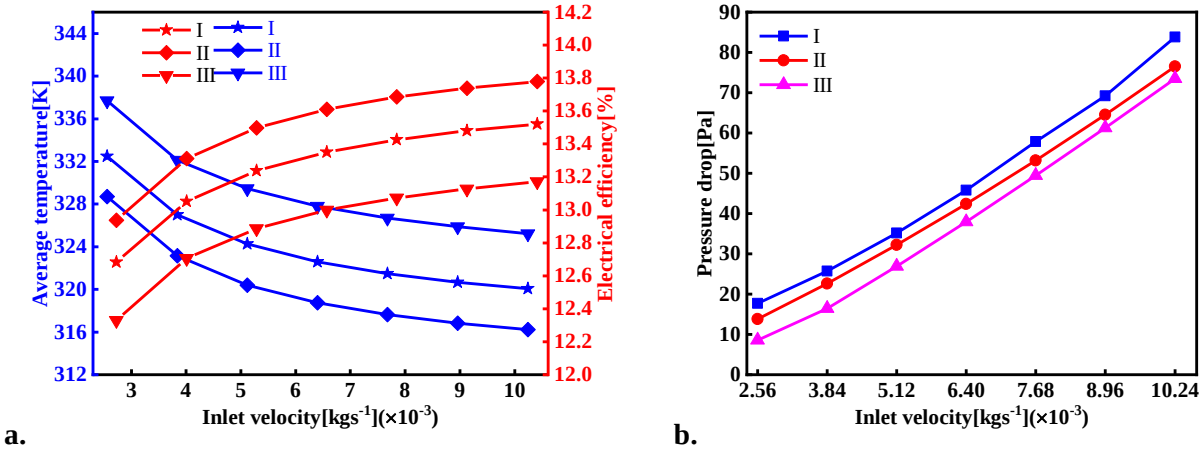

Figure 4 The variation of the a. T_{cell} and η_e and b. $\triangle P$ with the different cooling channel structures.

Figure 4 describes the effect of different bifurcating tree-like cooling channels on T_{cell}, η_e and ΔP for different inlet mass flow rate. As shown in Figure 4(a), for the II-type channel, the T_{cell} is the lowest and the η_e is the maximum. For the III-type channel has the highest T_{cell} and the lowest η_e. In particular, with increasing mass flow rate the decrease in T_{cell} and the increase in η_e slowed down. Under consistent boundary conditions, the convective thermal transfer is proportionate to the surface zone of the microchannel structure subjected to a flowing fluid. Moreover, the III-type generates a large thermic gradient which seriously affects the heat stability of the system. For the II-type channel, the average heat distribution on the PV module surface is very uniform, and thus the reduction of the temperature gradient effectively avoids the hazards brought about by the high local heat load of the PV module. Therefore, the nature-inspired bifurcating tree-like II-type cooling channel works best and the system of electrical performance is optimal. Moreover, the III-type generates a larger temperature gradient on the PV/T collector which weakness the reliability of the PV modules. For the II-type channel, the temperature distribution of the PV module surface is very uniform, and thus the reduction

of the temperature gradient effectively avoids the thermal runaway risks caused by the high local heat load of the PV module. Therefore, the nature-inspired bifurcating tree-like II-type cooling channel performs best and the electrical performance of the PV modules is optimal. As shown in Figure 4(b), by increasing the inlet flow speeds, the ΔP within the channel escalates. At equal inlet mass flow rate, the pressure drop of I-type channels exceeds that in II-type and III-type channels. With the increase in speed, the local resistance and frictional pressure drop in the cooling channel also rise. Furthermore, the ΔP in the cooling channel is mainly influenced due to friction, it's not merely dependent on the velocity of flow within the channel, but also the angle of the bifurcation and the length of the flow path. In particular, the I-type channel with maximum bifurcation angle, where the fluid impacts the wall causes the largest local resistance pressure drops. As the angles of the bifurcating tree-like channels in the III-type are much smaller than the I-type and II-type channels, and the III-type channel has the shortest runner length the pressure drop in the III-type channel is smallest. Therefore, the nature-inspired bifurcating tree-like II-type cooling channel works best and the system of electrical performance is optimal.

3.2. Effect of inlet flow-rates

The variation of the inlet speed directly influences the flow properties of the water through the bifurcating tree-like cooling channels and the efficiency of the systems. Accordingly, this section discusses the impact of flow rates on the PV/T collector with bifurcating tree-like II-type cooling channels.

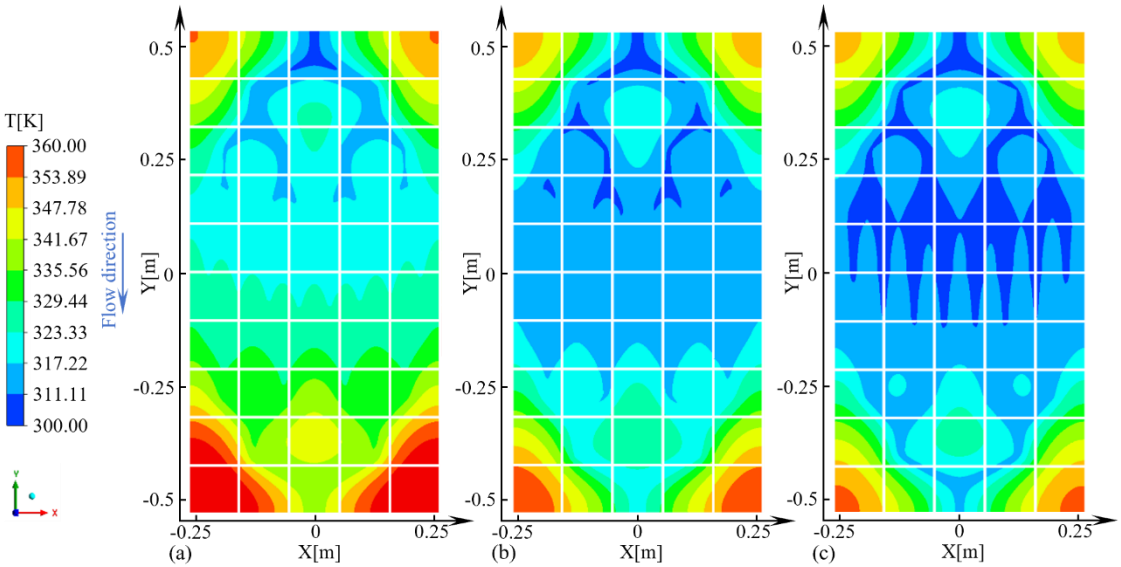

Figure 5 The distribution of temperature of PV modules with different inlet speeds.

Figure 5 illustrates the PV module surface temperatures at inlet mass flow rate of 0.00256, 0.0064, and 0.01024 kg/s. The temperature in the vicinity of the inlet is less than the outlet. Furthermore, with the rise of the v_{in} the high-temperature region on the surface of the PV module is gradually approaching the corners, and the cryogenic area is mostly found at the bifurcation in the cooling channel, which is particularly noticeable in Figure 5(c), and this phenomenon is more significant with speed rises. As the inlet speed gradually enhances 0.00256-0.01024 kg/s, the maximum temperature of the surface of the PV module is observed to decrease 376.91-355.71 K, and the minimum temperature decreases 304.44-303.30 K. As the v_{in} increases, the thermal transfer coefficient between the fluid and

the solids increases to improve the thermal transport effect. However, the cooling fluid is gradually heated by the PV module as it moves from inlet to outlet, and the temperature gradually rises, thus reducing the thermal transfer efficiency. And the vortex forms in the outer wall of the cooling channels, which will destroy the flow boundary layer and promotes the heat transfer between wall and the fluid nearby. Thus, there is larger areas in the cooling channel bifurcation with lower temperature, which is particularly noticeable in Figure 5(b). Therefore, the overall cooling effect of the PV module is relatively better as the mass flow rate at the inlet of the cooling channel increases from 0.00256 to 0.01024 kg/s, but the trend of change gradually diminishes.

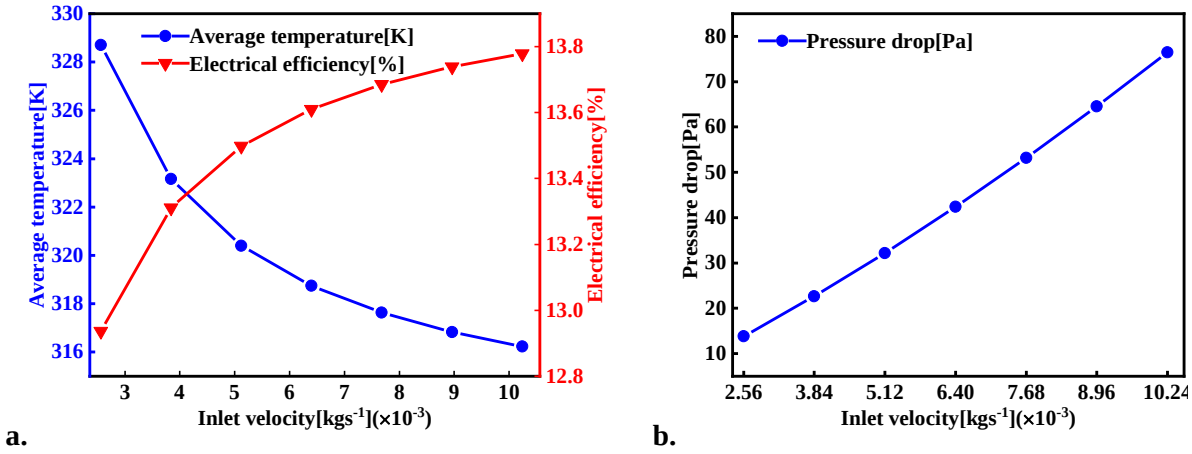

Figure 6 The variation of the a. T_{cell} and η_e and b. $\triangle P$ with the inlet mass flow rate speed.

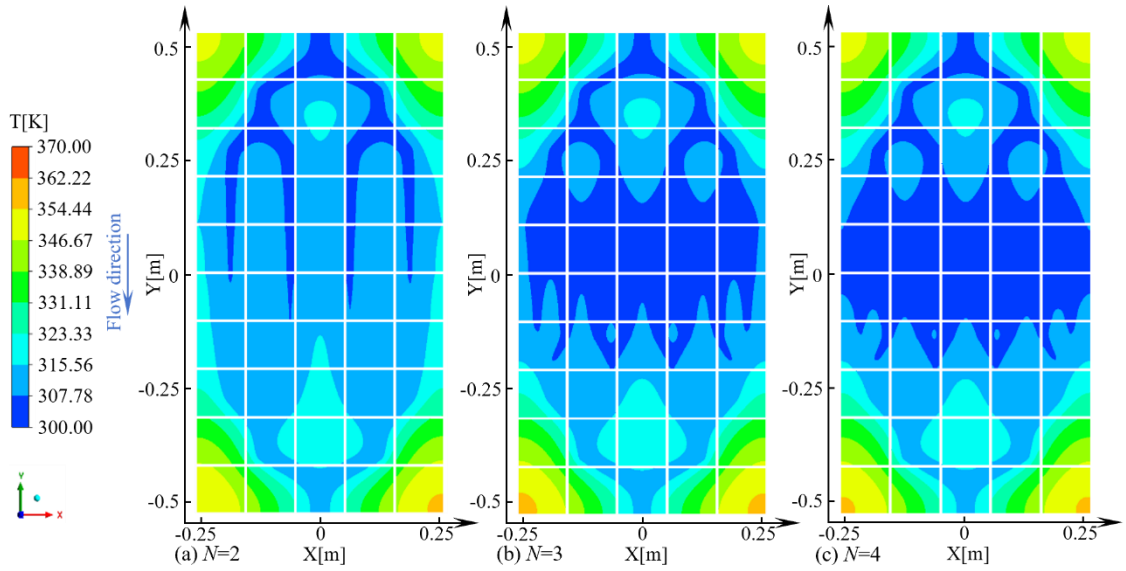

Figure 7 The distribution of temperature of PV modules with different numbers of gradings.

Figure 6 illustrates the variation of T_{cell}, η_e and $\triangle P$ with the inlet speed. As shown in Figure 6(a), the T_{cell} gradually reduces 328.71-316.24 K as the inlet flow speed increases. Besides, the η_e increases with the rise of the inlet speed 12.94-13.78%. Also, the magnitude of the changes in the T_{cell} and the η_e gradually decreases with the rise of the inlet speed. This assertion is supported by the consideration that when the speed in the cooling channel is low, the contact duration between the water and cooling channel thermal transfer surface is long and the thermal transfer coefficient is low, and vice versa. Besides, the fluid with a faster speed can carry out a thicker thermal boundary layer, which

makes it easier to facilitate better contact with the thermal transfer surface and improve the thermal transfer rate. As the flow speed rises, the direction of fluid flow along the channel changes continuously, which in turn disturbs the boundary layer and prevents it from thickening, further enhancing the heat dissipation effect. However, combined with Figure 6(b). As the v_{in} increases the $\triangle P$ in the cooling channel takes the form of an increasing curve. This phenomenon can be explained by the characteristics of the bifurcating tree-like cooling channels network structure, which is that the secondary flow generated at the bifurcation causes an additional pressure loss. Moreover, the flow in the channel is mainly affected by the $\triangle P_{\mathrm{f}}$ and $\triangle P_{\mathrm{lr}}$. With the rise in the inlet speed, the fluid collision cooling channels, and the formation of vortex energy loss rises. Also, the $\triangle P_{\mathrm{f}}$ and $\triangle P_{\mathrm{lr}}$ are strongly correlated with speed. Therefore, when the inlet mass flow rate is 0.01024 kg/s, the electrical efficiency of the system is the highest, and the pressure drops as the speed of the fluid rises.

3.3. Effects of numbers of gradings

The size of the cooling area is determined by the number of cooling channels graded. The difference in the cooling area directly affects the electrical efficiency of the PV/T collector within the cooling channels. Therefore, this section selects the cooling channels with the number of gradings 2, 3 and 4, also examines the impact of the number of gradings on the performance of the PV/T collector.

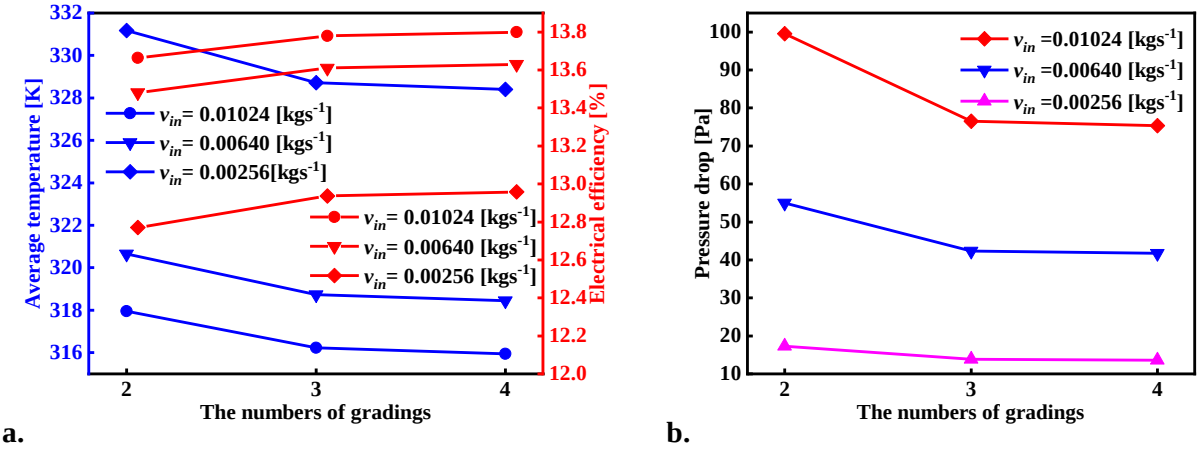

Figure 8 The variation of the T_{cell} and η_{e} and b. $\triangle P$ with the number of gradings.

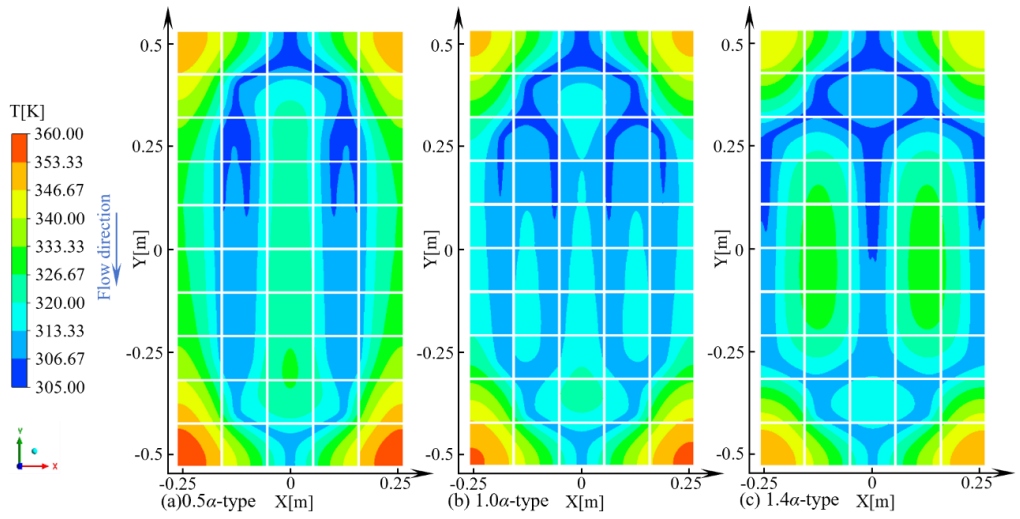

Figure 9 The distribution of temperature of PV modules at different channel bifurcation angles.

Figure 7 illustrates the distribution of the surface temperature of the PV module when the v_{in} is 0.01024 kg/s. With the rise in the number of gradings, the high-temperature regions change insignificantly. Besides, the max temperature reduces gradually as the number of stages rises, from 355.71 K at N = 2 to 355.17 K at N = 4. In particular, for different graded numbers of cooling channels, the corners of PV module's are hard to cooled sufficiently, thus the temperature distribution near the outlet of PV module is not uniform. More importantly, the low-temperature region expands considerably with the number of classifications. The laminar boundary layer has a small flow velocity, which can be equivalent to thermal conductivity. Thus, the thinner the boundary layer, the more favorable the heat transfer. Additionally, as the number of gradings rises, so does the count of bifurcations in the cooling channels and the instances of boundary layer disruptions. Therefore, when the N is 4, the improved thermal transfer performance in the channel results in better thermal uniformity.

Figure 8 illustrates the changes in T_{cell}, η_e and $\triangle P$ with the number of grades. As shown in Figure 8(a), as the rise in the number of grades, the change amplitude of the T_{cell} and the η_e reduces, while the change of the speed at the same number of grades has a more significant effect on it. For the number of grading is 4, the thermal is taken out of the PV module gradually increases and the cooling effect is gradually enhanced. Combined with Figure 8(b), under the same v_{in}, the pressure drops decrease gradually with a rising number of grades. However, when the N is 2, the $\triangle P_f$ along the flow path dominates, under these conditions, resulting in an increase in the $\triangle P_f$ along the flow path as the speed increases. Furthermore, when N = 4, the value of $\triangle P_{lr}$ is greater than the $\triangle P_f$, and as the number of grades rises, the flow speed within the cooling channel decreases, achieving the minimum pressure drop at 4 grades. Thus, the pressure loss in the cooling channel is maximum when N = 2 and v_{in} = 0.01024 kg/s.

3.4. Effect of channel bifurcation angles

The angle of the channel bifurcating tree-like markedly influences the comprehensive thermal transfer properties of the cooling channel. Common bifurcation angles for channels include the 0.5α-type, 1.0α-type and 1.4α-type (α = 87.38°). This section will delve into cooling channels with varying bifurcation angles to examine the main factors affecting of PV/T collector.

Figure 9 illustrates the PV module surface temperature at various channel bifurcation angles. The high-temperature region gradually approaches and shrinks toward the corners of the channel inlet and outlet when the channel bifurcation angle increases from 0.5α to 1.4α. Besides, the largest area of low-temperature regions when the bifurcation angle is of the 1.4α-type. As the bifurcation angle gradually increases, the maximum temperature decreases from 379.42 K for the 0.5α-type channel to 352.37 K for the 1.4α-type channel. This phenomenon can be attributed to the rise of the channel bifurcation angle, which slows down the central axial velocity, and leads to a backflow. It will disrupt the flow boundary layer, reducing its thickness and thereby enhancing heat transfer between the wall and the adjacent fluids. But it will also increase the flow resistance and the pressure drop of the cooling channel.

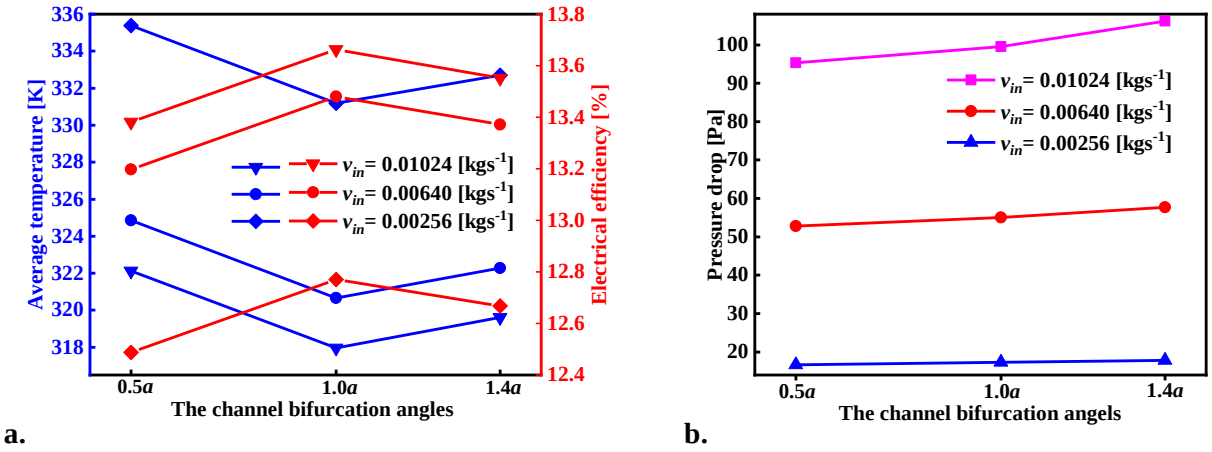

Figure 10 The variation of the a. T_{cell} and η_e and b. $\triangle P$ with the different bifurcation angles.

Figure 10(a) illustrates the impact of the channel bifurcation angles on the T_{cell} and η_e. The T_{cell} first diminishes and then increases as the channel bifurcation angle increments. Besides, the trend of the η_e increases and then decreases. Specifically, with the inlet mass flow rate at 0.01024 kg/s and the channel bifurcation angle at 1.0α-type, the T_{cell} is a minimum of 317.96 K, the η_e is a maximum of 13.66%, and when the channel bifurcation angle is 0.5α, the T_{cell} is a maximum of 322.13 K, and the η_e is a minimum of 13.38 %. More importantly, the channel bifurcation angle is too small or too large resulting in good localized cooling, but the overall thermal distribution is not uniform. Therefore, the PV/T collector featuring 1.0α-type cooling channels exhibits peak performance. Figure 13(b) illustrates the effect of different channel bifurcation angles on the $\triangle P$. The increase in channel bifurcation angle at lower inlet flow rates has less effect on the $\triangle P$ at the cooling channel. Under these conditions, the $\triangle P_{lr}$ dominates. As the channel bifurcation angle increases, the phenomenon of fluid impacting the bifurcating cooling channel and then forming a backflow on the outer wall surface of the channel becomes more intense, increasing the $\triangle P_{lr}$. Thus, the 0.5α-type cooling channel has the maximum $\triangle P$.

In summary, the structural parameters of the cooling channels significantly influence the electrical efficiency of the PV/T collector system. Figure 11 illustrates that the electrical efficiencies simulated in this study are in agreement with the ranges in other studies[15, 26-30], which confirms the reliability and superiority of the results.

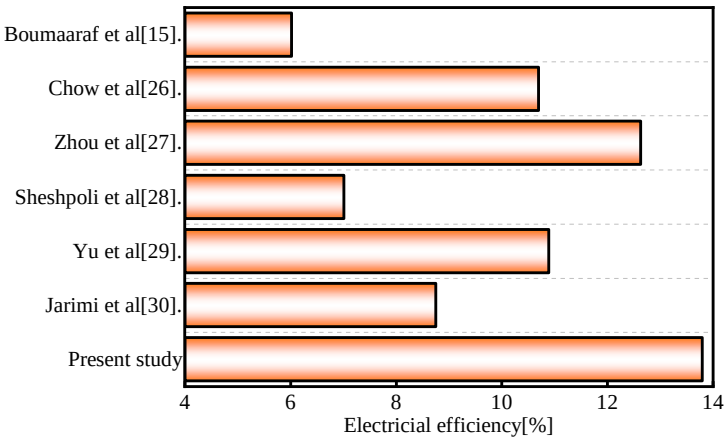

Figure 11 Comparison of current simulation results with other studies.

4. Conclusions

To decrease the mean surface temperature of the PV module and improve the efficiency of the PV/T collector, this study designs bifurcating tree-like cooling channels. By constructing the thermal transport steady-state model, the characteristics of thermal transfer and the impact on the performance of the systems by the nature-inspired bifurcating tree-like cooling channels are systematically compared with the traditional parallel cooling channels. The fundamental thermal transfer mechanism in the bifurcating tree-like cooling channel is elucidated.

To summarize, the major conclusions are as follows: by comparing traditional parallel cooling channels and bifurcating tree-like cooling channels. The $\triangle P$ with III-type cooling channel is more than 10% lower than with II-type and I-type. The T_{cell} of the PV module is about 3% or less than the I-type and III-type, and the η_e is higher than that of I-type and III-type by about 2.5% or more when the cooling channel grading structure is II-type. Hence, the bifurcating tree-like II-type cooling channel offers a greater advantage. Besides, the rise in v_{in} improves the performance of the PV/T collector, but the $\triangle P$ inside the tube is also elevated. Specifically, increasing the v_{in} from 0.00256 to 0.01024 kg/s reduces the PV module surface temperature by 12.47 K and raises the electrical efficiency by 0.84%. Furthermore, with the increase in the number of grades, the $\triangle P$ within the bifurcating tree-like cooling channels progressively diminishes, the η_{e} increases consistently, and the average surface temperature of the PV module decreases accordingly. Therefore, considering the trade-offs between pressure drop loss and production cost, N = 2 is the most appropriate choice. However, to maximize the total performance of the system, N = 4 is preferable. Moreover, as the bifurcation angles increase, the PV modules of 0.5α-type and 1.4α-type have an average temperature that is over 1.5 K higher and the η_{e} that is more than 0.1% lower compared to the 1.0α-type. In the 1.0α-type configuration, the temperature gradients on the PV module is minimal, which reduces the required pump power for heat dissipation while enhancing the performance of the PV/T collector as a whole.

In previous investigations of PV/T collectors with different cooling channels, the optimal design of the channels significantly improved the system performance, which is consistent with the conclusions in this paper. Moreover, comparison with related studies found that the bifurcating tree-like cooling channels further improved the performance of the PV/T collector. However, in practical engineering applications, the selection and design of the cooling channel should comprehensively consider the pressure drop loss in the cooling channel and its economic cost of processing and fabrication, which will be studied in our future work.

Acknowledgment

The authors are grateful for the support by National Natural Science Foundation of China (No. 92271111) and China Postdoctoral Science Foundation (Grant Number 2023M730556).

Nomenclature

$I_{b\lambda}$	-the blackbody emission in the wavelength band per unit solid angle	θ	-furcation angle, [°]
L	-length, [mm]	σ_λ	-spectral absorption coefficient
M	-the number of data	σ_s	-scattering coefficient
ΔP	-pressure drop, [Pa]	ψ	-transmittance
R_e	-Reynold	*Acronyms*	

T_{cell}	-the average PV module temperature, [K]	PV	-photovoltaic
W	-Weight, [mm]	PV/T	-photovoltaic/thermal
$X_{exp,i}$	-the experimentally obtained value	RMSE	-the root-mean-square deviation
$X_{sim,i}$	-the simulated value and represents	*Subscript*	
Greek		a*i*	-the subchannels of stages *i* of I-type
α	-absorption	b*i*	-the subchannels of stages *i* of II-type
ε	-emissivity	c*i*	-the subchannels of stages *i* of III-type
λ	-thermal conductivity, [$Wm^{-1}k^{-1}$]	in	-inlet
η_e	-photoelectric conversion efficiency, [%]	lr	-local resistance
η_{swc}	-standard condition photoelectric conversion efficiency, [%]	f	-frictional

References

[1] Ganesan, D., *et al.*, THERMAL STUDIES ON HEAT SINKS EXPOSED TO SOLAR IRRADIATION, *Thermal Science*, *28* (2024), 1A, pp. 1 - 12

[2] Hissouf, M., *et al.*, Analysis of the exergy performances of a glazed and unglazed PV/T collector under different conditions, *International Journal of Heat and Mass Transfer*, *226* (2024), p. 125447

[3] Umar, M., *et al.*, A stochastic computing procedure to solve the dynamics of prevention in HIV system, *Biomedical Signal Processing and Control*, *78* (2022), p. 103888

[4] Irem, K.,M. Tayfun, Numerical study of a photovoltaic thermal (PV/T) system using mono and hybrid nanofluid, *Solar Energy*, *224* (2021), pp. 1260-1270

[5] Alami, Y.E., *et al.*, Numerical study of a water-based photovoltaic-thermal (PVT) hybrid solar collector with a new heat exchanger, *e-Prime - Advances in Electrical Engineering, Electronics and Energy*, *9* (2024), p. 100693

[6] Kharaz, H.E., *et al.*, A numerical analysis of air flow topology within a vertical channel attached behind photovoltaic panel, *International Journal of Heat and Mass Transfer*, *223* (2024), p. 125254

[7] Arslan, E., *et al.*, Numerical and experimental assessment of a photovoltaic thermal collector using variable air volume, *Thermal Science and Engineering Progress*, *39* (2023), p. 101735

[8] El Alami, Y., *et al.*, Solar thermal, photovoltaic, photovoltaic thermal, and photovoltaic thermal phase change material systems: A comprehensive reference guide, *International Communications in Heat and Mass Transfer*, *159* (2024), p. 108135

[9] El Alami, Y., *et al.*, Performance evaluation of different new channel box photovoltaic thermal systems, *Journal of Cleaner Production*, *478* (2024), p. 143953

[10] Kong, D., *et al.*, Experimental study of solar photovoltaic/thermal (PV/T) air collector drying performance, *Solar Energy*, *208* (2020), pp. 978-989

[11] Faruk Can, Ö., *et al.*, Experimental and numerical assessment of PV-TvsPV by using waste aluminum as an industrial symbiosis product, *Solar Energy*, *234* (2022), pp. 338-347

[12] Bošnjaković, M., *et al.*, BUILDING INTEGRATED PHOTOVOLTAICS. OVERVIEW OF BARRIERS AND OPPORTUNITIES, *Thermal Science*, *27* (2023), 2B, pp. 1433 - 1451

[13] Candanedo, L., *et al.*, *NUMERICAL MODELLING OF HEAT TRANSFER IN PHOTOVOLTAIC-THERMAL AIR BASED SYSTEMS, 3rd Canadian Solar Buildings Conference*. 2008: Fredericton, NB, Canada. p. 180-188.

[14] Shen, C., *et al.*, A numerical investigation on optimization of PV/T systems with the field

synergy theory, *Applied Thermal Engineering*, *185* (2021), p. 116381
[15] Boumaaraf, B., *et al.*, Comparison of electrical and thermal performance evaluation of a classical PV generator and a water glazed hybrid photovoltaic–thermal collector, *Mathematics and Computers in Simulation*, *167* (2020), pp. 176-193
[16] Wang, J., *et al.*, Design and experimental study of a novel flexible PV/T structure, *Energy*, *296* (2024), p. 131139
[17] Poredoš, P., *et al.*, Numerical and experimental investigation of the energy and exergy performance of solar thermal, photovoltaic and photovoltaic-thermal modules based on roll-bond heat exchangers, *Energy Conversion and Management*, *210* (2020), p. 112674
[18] Nahar, A., *et al.*, Numerical and experimental investigation on the performance of a photovoltaic thermal collector with parallel plate flow channel under different operating conditions in Malaysia, *Solar Energy*, *144* (2017), pp. 517-528
[19] Shen, C., *et al.*, Numerical study on the thermal performance of photovoltaic thermal (PV/T) collector with different parallel cooling channels, *Sustainable Energy Technologies and Assessments*, *45* (2021), p. 101101
[20] Dong, S., *et al.*, Performance investigation of a hybrid PV/T collector with a novel trapezoidal fluid channel, *Energy*, *288* (2024), p. 129594
[21] Kong, X., *et al.*, Numerical Study on the Optimization Design of Photovoltaic/Thermal (PV/T) Collector with Internal Corrugated Channels, *International Journal of Photoenergy*, *2022* (2022), p. 101101
[22] Xing, Y., *et al.*, Formation of bionic surface textures composed by micro-channels using nanosecond laser on Si3N4-based ceramics, *Ceramics International*, *47* (2021), 9, pp. 12768-12779
[23] Waqas, H., *et al.*, Numerical and Computational simulation of blood flow on hybrid nanofluid with heat transfer through a stenotic artery: Silver and gold nanoparticles, *Results in Physics*, *44* (2023), p. 106152
[24] Azeem, S., *et al.*, Thin film flow and heat transfer of Cu-nanofluids with slip and convective boundary condition over a stretching sheet, *Scientific Reports*, *12* (2022), 1, pp. 14254-14254
[25] Madhi, H., *et al.*, Comparative numerical study on the effect of fin orientation on the photovoltaic/thermal (PV/T) system performance, *International Journal of Thermofluids*, *24* (2024), p. 100909
[26] Chow, T.T., *et al.*, Hybrid photovoltaic-thermosyphon water heating system for residential application, *Solar Energy*, *80* (2006), 3, pp. 298-306
[27] Zhou, J., *et al.*, Clear-days operational performance of a hybrid experimental space heating system employing the novel mini-channel solar thermal & PV/T panels and a heat pump, *Solar Energy*, *155* (2017), pp. 464-477
[28] Zabihi Sheshpoli, A., *et al.*, Numerical and experimental investigation on the performance of hybrid PV/thermal systems in the north of Iran, *Solar Energy*, *215* (2021), pp. 108-120
[29] Yu, Y., *et al.*, Testing and modelling an unglazed photovoltaic thermal collector for application in Sichuan Basin, *Applied Energy*, *242* (2019), pp. 931-941
[30] Jarimi, H., *et al.*, Bi-fluid photovoltaic/thermal (PV/T) solar collector: Experimental validation of a 2-D theoretical model, *Renewable Energy*, *85* (2016), pp. 1052-1067

Paper submitted: 03.11.2024
Paper revised: 12.12.2024
Paper accepted: 20.12.2024